Int J Fract
https://doi.org/10.1007/s10704-024-00820-4

RESEARCH

How to measure fracture toughness of soft materials: a comparison of six different approaches using blood clot as a model material

Matthew J. Lohr · Grace N. Bechtel · Berkin Dortdivanlioglu · Manuel K. Rausch

Received: 5 August 2024 / Accepted: 18 November 2024

Abstract Soft materials are an important class of materials. They play critical roles both in nature, in the form of soft tissues, and in industrial applications. Quantifying their mechanical properties is an important part of understanding and predicting their behavior, and thus optimizing their use. However, there are often no agreed upon standards for how to do so. This also holds true for quantifying their fracture toughness; that is, their resistance to crack propagation. The goal of our work is to fill this knowledge gap using blood clot as a model material. In total, we compared three general approaches, some with multiple different implementations. The first approach is based on Griffith's definition of the critical energy release rate. The second approach makes use of the J-Integral. The last approach uses cohesive zones. We applied these approaches to 12 pure shear experiments with notched samples (some approaches were supplemented with unnotched samples). Finally, we compared these approaches by their intra- and inter-approach variability, the complexity of their implementation, and their computational cost. Overall, we found that the simplest method was also the most consistent and the least costly one: the Griffith-based approach, as proposed by Rivlin and Thomas in 1953.

Keywords Pure shear · Mode I · Griffith · Cohesive zones · J-integral · Critical energy release rate

Mathematics Subject Classification 0000 · 1111

Supplementary Information The online version contains supplementary material available at https://doi.org/10.1007/s10704-024-00820-4.

M. J. Lohr · G. N. Bechtel · M. K. Rausch
Department of Biomedical Engineering, The University of Texas at Austin, 107 W Dean Keeton St, Austin, TX 78712, USA

B. Dortdivanlioglu
Department of Civil, Architectural & Environmental Engineering, The University of Texas at Austin, 301E E Dean Keeton St, Austin, TX 78712, USA

B. Dortdivanlioglu · M. K. Rausch (✉)
Oden Institute for Computational Engineering and Sciences, The University of Texas at Austin, 201 E 24th St, Austin, TX 78712, USA
e-mail: manuel.rausch@utexas.edu

M. K. Rausch
Department of Aerospace Engineering & Engineering Mechanics, The University of Texas at Austin, 2617 Wichita St, Austin, TX 78712, USA

M. K. Rausch
Department of Mechanical Engineering, The University of Texas at Austin, 204 E Dean Keeton, Austin, TX 78712, USA

1 Introduction

Soft materials are ubiquitous in nature and widely popular in many engineering disciplines. In nature, soft materials are found as soft tissues such as skin, muscles, brain, and internal organs (Fung 1993). In engineering, they are used in biomedical applications such as tissue engineering (Slaughter et al. 2009; Lee and Mooney

Published online: 13 January 2025

2001), drug delivery (Peppas et al. 2006), implantable devices (Yoda 1998; Robinson et al. 2024), and wearable electronics (Kim et al. 2011; Nassar et al. 2016), as well as industrial applications such as ionic conductors (Yang et al. 2015), soft robotics (Xu et al. 2022), and food products (McClements et al. 2009). As their name suggests, they are significantly softer than traditional engineering materials with stiffnesses ranging on the order of Pa - MPa (Chen et al. 2017; Varner et al. 2023), rather than MPa - GPa as seen in metals and ceramics (Piggott 1975). Albeit they provide a myriad possibilities and are suitable for many applications, soft materials also pose significant downsides. For example, their often complex composition and inhomogenous microstructure give rise to a wide range of mechanically challenging phenomena that are difficult to measure, model, and predict. Such phenomena include viscoelasto-plasticity(Slaughter et al. 2009; Crespo-Cuevas et al. 2023), anisotropy (Perez-Puyana et al. 2020), heterogeneity (Stano and Percoco 2021), Mullins-type damage (Mullins 1969), active contraction and swelling (Zhou et al. 2015; Shur et al. 2023; Dortdivanlioglu and Linder 2019), surface effects (Style et al. 2017; Ang et al. 2020; Dortdivanlioglu and Javili 2021; Rastogi and Dortdivanlioglu 2022), and complex instabilities (Wang and Zhao 2015; Dortdivanlioglu and Javili 2022).

Subject to this manuscript is another complex aspect of soft material mechanics, their fracture behavior. That is, soft materials may fail at very – sometimes extremely – large deformations (Sun et al. 2012; Zhu et al. 2024), rendering them unsuitable for analyses using classic linear fracture mechanics (Knowles and Sternberg 1973). Understanding and predicting the fracture behavior of soft materials is therefore a formidable problem. Often, a first goal in studying soft material fracture is to determine a material's fracture toughness, that is, their resistance to crack propagation. For example, in our work on blood clots – a prototypical soft (biological) material – we have been interested in measuring fracture toughness as a determinant of a clot's resistance to breaking off from its original site of formation (Sugerman et al. 2023; Gültekin et al. 2024; Sugerman et al. 2024). As such, it is a critical determinant of many devastating diseases, including strokes, heart attacks, and pulmonary embolisms (Wendelboe and Raskob 2016). Having the ability to quantify fracture toughness and predict the fracture behavior of blood clots is therefore of significant clinical importance.

As we first set out to measure the fracture toughness of blood clot, we found that there are no agreed upon best practices. Instead, we found a number of approaches that differed fundamentally in their complexity and (computational) cost. To the best of our knowledge, there are no prior comprehensive comparisons of these approaches, especially not for soft biological materials, such as blood clot. The main goal of our work is to test and directly compare established approaches to quantify the fracture toughness of soft materials. Please note that blood clot – as so many other soft materials – is a complex material due to its composition. Blood clot is comprised 50% of a fluid phase, as well as passive fillers (red blood cells), active fillers (platelets), and a semi-flexible biopolymer backbone (Qiu et al. 2019). This complexity gives rise to several confounding (dissipative) phenomena that complicate the determination of fracture toughness, including damage (Sugerman et al. 2020), viscoelasticity, and poroelasticity (Ghezelbash et al. 2022). For the purpose of this work, we, like others before us, ignore these complexities as a first approximation of clots fracture behavior (Fereidoonnezhad et al. 2021a, b; Luraghi et al. 2021a, b; Mousavi et al. 2021).

In detail, we identified three general approaches to measuring fracture toughness, some with alternative implementations. These approaches are as follows: The *Griffith* approaches based on Griffith's fracture criterion (Griffith 1921), the *J-Integral* approach based on work by Rice (Rice 1968), and the *cohesive zone* approach based on the work by Dugdale and Barenblatt (Dugdale 1960; Barenblatt 1962). Here, we would like to note that previous work has established that Griffith's approach and the J-integral are equivalent, even in hydrated, soft materials (Bouklas et al. 2015). In each approach, we use experimental data from traditional notched and unnotched pure shear experiments, but note that other geometries can and have been used (Fereidoonnezhad et al. 2021a; Liu et al. 2021; Tutwiler et al. 2020; Gültekin et al. 2024; Ramanujam et al. 2024). We note that, when loaded under tension, blood clots may expel some fluid, rendering them not fully incompressible (Garyfallogiannis et al. 2023). Thus, our experiments may violate the assumptions of pure shear experiments. Our use of the term "pure shear" should therefore be viewed under this limitation; we expand on this in our Discussion.

Moreover, we note that we limit ourselves to determining fracture toughness under Mode I loading as is customary in soft materials undergoing large deformation (Zhu et al. 2024). After introducing each approach, we will compare and judge these approaches according to their intra- and inter-approach variability, the difficulty of their implementation, and their computational cost. Emerging techniques, such as mapping crack tips (Qi et al. 2019) and capturing crack front geometry (Wei et al. 2024), which play important roles in fracture toughness, require advanced and sometimes scarcely available instrumentation, and are therefore beyond the scope of this work.

2 Methods

2.1 Pure shear and mode I fracture experiments

In our work, we first created blood clots in pure shear geometry (40 x 10 x 3 mm) from human blood. Specifically, we collected blood from one human subject via venipuncture following a protocol approved by our local Institutional Review Board. Then, we prepared samples according to previously published protocols (Sugerman et al. 2021). That is, we initiated coagulation by adding calcium chloride to the blood at a concentration of 20 mM to reverse the acid citrate dextrose (ACD) anticoagulant. Next, we added the blood to a 3D-printed mold where it fully coagulated for 60 min at 37^oC. Note, the molds were lined with Velcro to create a secure attachment between the blood clot and testing fixture. Before mounting the samples to our uniaxial tensile tester (Instron 5943, 10 N load cell), we speckled the samples with a mix of black and white sand for use with digital image correlation (DIC). For details on speckle size, mean image gradient, and other measures of speckle quality, please see our recent publication on the subject (Sugerman et al. 2023). All experiments were approved by our local Institutional Review Board.

In total, we produced 15 samples. Three samples were tested "as are," while 12 samples received lateral notches with unique lengths ranging from $3.5-17$ mm. These notches were introduced using a razor blade. Upon mounting the samples, the crack tip rounded. We extended all pure shear samples at a rate of 0.1 mm/s which, at a sample height of 10 mm, translates to a strain rate of approximately 1 %/s. During testing, we measured time, displacement, and force. We also took images of the samples using a digital camera. During post-processing, we used the open source software NCORR (www.ncorr.com) to convert speckle images into strain maps via DIC (Blaber et al. 2015). Note, we optimized the DIC algorithmic parameters via sensitivity studies before our final analysis. Figure 1 shows a summary of the data from the unnotched and notched pure shear experiments, while Fig. 2 shows example images of a notched sample as well as results from DIC. Please see Supplementary Table S1 for a list of all samples and their notch lengths as well as their critical displacements and Supplementary Table S2 for a list of all NCORR parameters used during the digital image correlation analysis.

2.2 Hyperelastic model

In approaches *Griffith B, J-Integral*, and *cohesive zone*, we required capturing the elastic behavior of our samples in a constitutive model. To this end, we assumed that blood clot acts as a hyperelastic, incompressible, one-term Ogden material (Ogden 1972; Sugerman et al. 2021; Lohr et al. 2022). The strain energy density per reference volume of the Ogden model reads

$$W = \frac{2\mu}{\alpha^2}(\lambda_1^\alpha + \lambda_2^\alpha + \lambda_3^\alpha - 3) + U(J). \tag{1}$$

Here, μ is the shear modulus, α dictates the strain-stiffening behavior, which we informed through inverse finite element analyses using Abaqus/Implicit (6.20-1, Dassault Systémes, Vélizy-Villacoublay, France). Abaqus's implementation of the Ogden model, which is formulated in its compressible form, adds the volumetric energy term, $U(J) = \frac{1}{D}(J-1)^2$. Here, $J = \lambda_1\lambda_2\lambda_3$ is the determinant of the deformation gradient. In our work, we approximate blood clot as an incompressible material. To this end, we effectively treated the bulk modulus, $\kappa = \frac{2}{D}$, as a penalty by selecting it to be three orders of magnitude larger than the shear modulus, μ (Li et al. 2015). In contrast, in our analytical approaches, we used the Lagrange multiplier method, in which we define $U(J) = p(J-1)$, and analytically solve for p to perfectly enforce incompressibility.

For our inverse finite element analysis, we first modeled each sample's geometry (including its specific notch length) exactly using 15000-22000 linear plane stress quadrilateral elements (Abaqus element CPS4R).

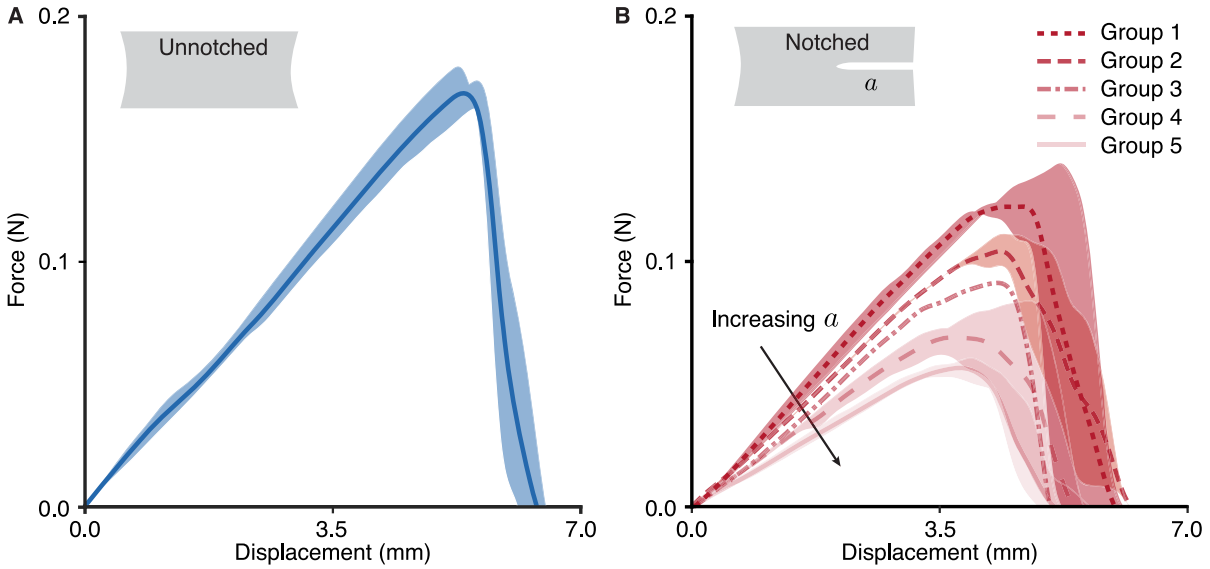

Fig. 1 Summary of mechanical test data. **A** Force-displacement data from three unnotched pure shear experiments showing mean ± 1 standard deviation. **B** Force-displacement data from 12 notched pure shear experiments, again showing mean ± 1 standard deviation. We grouped/binned the 12 samples according to their notch size with Group 1-5 having average notch sizes of 3.7, 7.3, 9.7, 11.9, and 16.5 mm, respectively. See Supplementary Table S1 for a list of all sample geometries

Please note that for all models, we used a crack tip radius of 0.25 mm. We performed a careful sensitivity study to assess the impact of crack tip radius on reaction force and fracture toughness. We found that both measures were insensitive to the radius within the tested range. We then iteratively conducted forward simulations to identify the Ogden parameters using a least-squares approach that minimized the difference between the experimentally measured and computationally predicted reaction forces. We limited the sample displacement to $\delta = 0.9\delta_c$ to constrain our analysis to the pre-fracture regime, where δ_c is the critical displacement at which crack initiation begins. We determined the critical displacement as the displacement corresponding to the onset of crack growth based on images of the crack tip taken during testing. Please note that we used a multi-start approach with random initial guesses to minimize the risk of identifying local minima. We repeated this process for each of our 12 notched samples and thus obtained 12 separate sets of material parameters. See Fig. 3 A for an example simulation result and Supplementary Table S3 for a list the material parameters of each sample.

2.3 Approach 1: the "Griffith" approach

Our first approach to estimating fracture toughness arises from Griffith's equation for the critical energy release rate G_c (Griffith 1921)

$$G_c = -\frac{\partial W(\lambda_c)}{\partial A}, \tag{2}$$

where W is the internal strain energy, $\lambda_c = 1+\delta_c/H$ is the critical stretch calculated using the sample's critical displacement, δ_c and the sample's original height, H, and A is the added surface area due to crack growth in the reference configuration. We term this the "Griffith" approach.

2.3.1 Griffith A: hybrid aproach

Our first implementation of this approach comes from Rivlin and Thomas's seminal work on rubber rupture (Rivlin and Thomas 1953). Under the assumptions of a perfectly elastic material in pure shear deformation, Rivlin and Thomas derived a simple formula based on

Eq. 2, which reads as

$$G_c = \frac{W(\delta_c)}{V} H_0. \tag{3}$$

Here again, $W(\delta_c)$ is the strain energy put into the unnotched sample up to the critical displacement, V is the sample volume, and H is the sample's initial height. Equation 3 assumes that the sample is long and that there is steady-state crack growth. Rivlin and Thomas derived this equation from the energy stored in the region of the material that is in a state of pure shear (Rivlin and Thomas 1953). To compute $W(\delta_c)$, we identified the critical displacement from the recorded images of each notched sample and then integrated and averaged the force and displacement data of each unnotched sample up to δ_c, see Fig. 4Ai-ii. Thereby, we obtained a separate G_c for each of our 12 notched samples.

2.3.2 Griffith B: numerical approach

In the second implementation of the *Griffith* approach, we again used Eq. 3 but instead determined $W(\delta)$ from the notched pure shear experiment using a numerical approach. That is, we simulated (Abaqus/Implicit, 6400 CPS4R) a pure shear experiment using the material parameters identified through our inverse finite element approach as described in Sect. 2.2. We then computed $W(\delta_c)$ again by integrating the (synthetic) data on the predicted force and displacement up to δ_c, see Fig. 4Ai-ii. Note, this approach did not require the unnotched pure shear sample data.

2.3.3 Griffith C: experimental approach

In the third implementation of the *Griffith* approach, we directly used Eq. 2 and approximated the partial derivative $\partial W(\delta_c)/\partial A$ from experimental data only (Roucou et al. 2015). That is, we calculated the fracture toughness as the change in W with increasing notch lengths using a finite difference scheme, where we computed W as the integral under the force-displacement curve between samples of differing notch lengths, see Fig. 4Aiii. To this end, we organized the 12 notched samples into five ordered groups with average notch lengths of 3.70, 7.33, 9.70, 11.90, and 16.51 mm, respectively, see Fig. 1 again for reference. Specifically, we used forward and backward differences to calculate ΔW and ΔA between adjacent groups. For the exterior groups we used either a forward or backward difference, and for the interior groups, we averaged the G_c value calculated using both differences. Note, this approach did not require the unnotched pure shear sample data and did not make use of simulation tools.

2.4 Approach 2: the "J-Integral" approach

The second approach to estimating fracture toughness arises from the definition of the J-integral. This counterclockwise contour integral around the notch is defined as follows using the traditional Einstein summation convention,

$$J = \int_\Gamma [W N_1 - P_{\alpha\beta} N_\beta \frac{\partial \delta_\alpha}{\partial x_1}] d\Gamma. \tag{4}$$

Here, N_1 is the normal vector to the contour, Γ, $P_{\alpha\beta}$ are the in-plane components of the first Piola-Kirchhoff stress tensor, δ_α are the in-plane displacement vectors, and x_1 is the direction parallel to the notch. Note that the J-integral is evaluated in the reference configuration. As such, the aforementioned tensors and vectors are reference quantities. The J-integral was first derived by Rice (Rice 1968). It has since been shown to be equivalent to G_c in nonlinear elastic materials (Long and Hui 2015).

2.4.1 J-Integral A

For our first implementation of this approach, we used DIC-derived full-field deformations to compute the J-integral. To this end, we used NCORR to compute the in-plane principle stretches and the displacement gradients, $\partial \delta_\alpha / \partial X_1$, at each sample material point. Next, we computed the first Piola-Kirchhoff stress as per

$$P_a = \frac{\partial W}{\partial \lambda_a} - \frac{p}{\lambda_a}, \tag{5}$$

where λ_a are the DIC-derived principle stretches, W is the strain energy, and p is the Lagrange multiplier that enforces incompressibility. Here we again assumed that our material behaved like an incompressible, one-term Ogden material and estimated W using the material parameters as identified in Sect. 2.2. Additionally, we analytically solved for p under the assumption of plane stress conditions. Finally, we computed

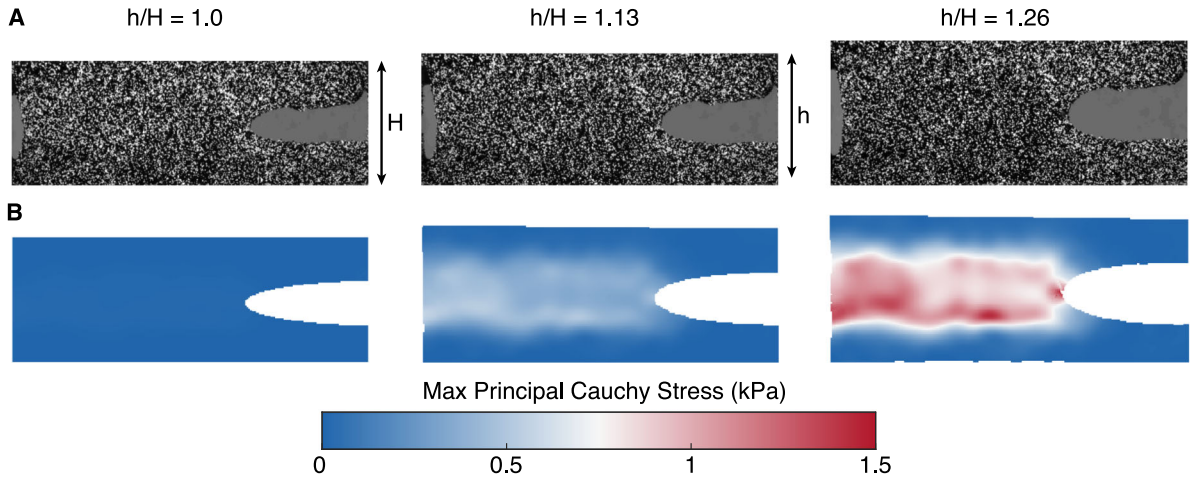

Fig. 2 Example imaging and digital image correlation data. **A** Images of a speckled and notched blood clot sample in the reference configuration and two levels of stretch. **B** Digital image correlation-based stress maps at the sample levels of stretch as in **A**

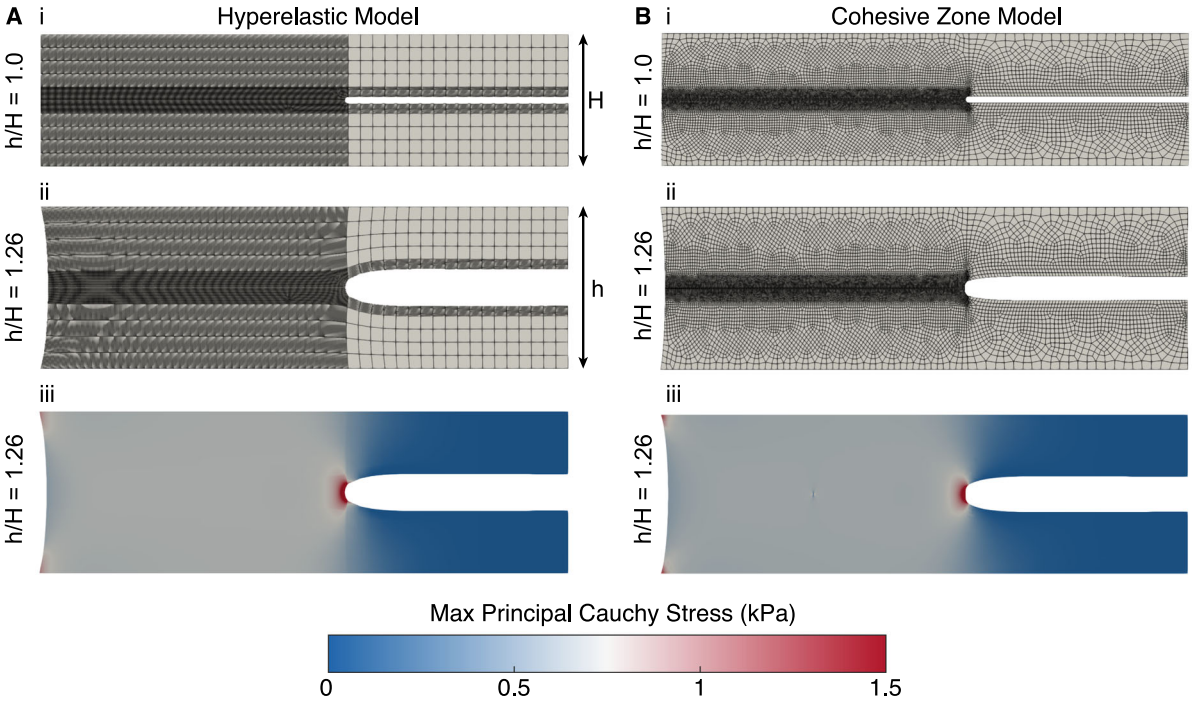

Fig. 3 Example results of finite element simulations. **A** A hyperelastic simulation of a notched sample discretized with 17823 Abaqus CPS4R elements. **B** A cohesive zone simulation of a notched sample discretized with 15975 Abaqus CPS4 elements, and 600 COH2D4 (cohesive) elements

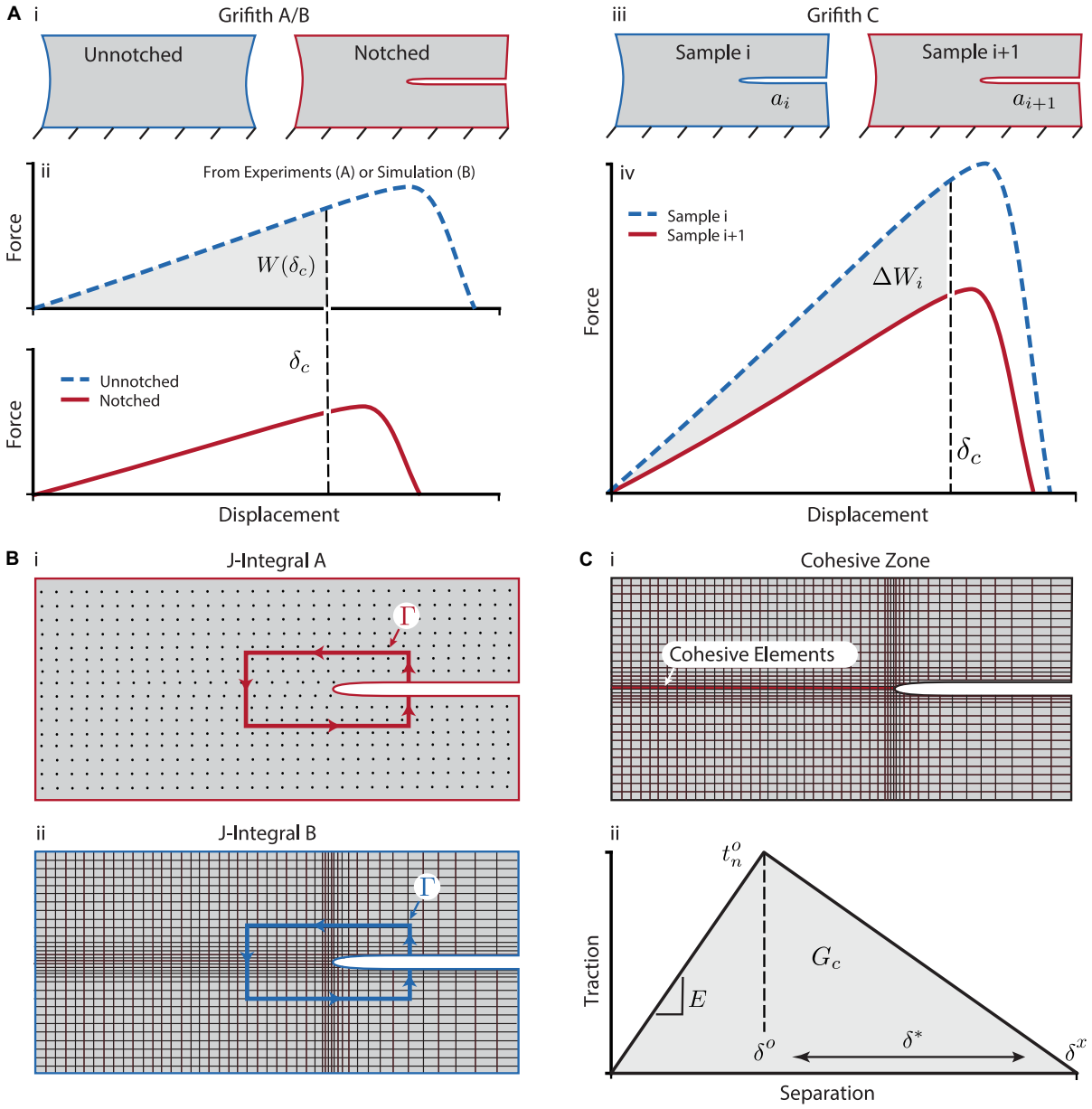

Fig. 4 Methodological overview of the *Griffith*, *J-Integral*, and *cohesive zone* approaches. **A**) *Griffith A* and *Griffith B* use Rivlin and Thomas' work in Eq. 3 to estimate the fracture toughness (i-ii), while *Griffith C* estimates fracture toughness directly from Eq. 2 (iii). Please note that $W(\delta_c)$ in (ii) is equivalent to $W(\lambda_c)$ in Eq. 2. **B**) *J-Integral A* computes the J-integral of Eq. 4 with the help of digital image correlation data (i), while *J-Integral B* uses simulation results and Abaqus' built-in J-Integral evaluator (ii). **C**) *cohesive zone* uses cohesive zone elements (i) with a bilinear traction-separation law (ii) to estimate fracture toughness

the *J-Integral* according to Eq. 4 using the DIC-derived kinematic data and the estimated stresses. For the actual integration, we drew rectangular contours that began and ended on the notch, far from the notch tip and sample boundaries, see Fig. 4Bi. We repeated this procedure for each of the 12 notched samples. Note, this approach did not require the unnotched pure shear sample data.

2.4.2 J-Integral B

For our second implementation of this approach, we used Abaqus' built-in J-integral function to evaluate Eq. 4. To this end, we simulated the pure shear experiments of each notched sample using a mesh with a highly refined region around the notch tip ($\sim$ 12000 CPS4R elements). See Fig. 3A for an example simulation. We then used Abaqus' built in J-Integral evaluator to compute the *J-Integral* at each samples δ_c, see Fig. 4Bii. We repeated this procedure for each of the 12 notched samples. Note, this approach did not require the unnotched pure shear sample data or DIC data.

2.5 Approach 3: the "*cohesive zone*" approach

The third and final approach to estimating fracture toughness arises from the work on cohesive zones that may be attributed to work by Dugdale and Barenblatt (Dugdale 1960; Barenblatt 1962). In this approach, we first implemented a finite element model of the notched pure shear experiments similar to what we did in the *Griffith* and *J-Integral* approaches; however, here, we defined a cohesive interface between the bottom and top halves of the pure shear geometry using cohesive elements (Abaqus elements COH2D4), see Fig. 3B for an example simulation and Fig. 4Ci for the location of the cohesive zone elements. For the bulk of the material, we used 15000-17500 CPS4 elements, while we used approximately 600 COH2D4 elements for the cohesive zone. We chose a height of 3 μm for our cohesive elements after a careful sensitivity study that showed no changes in the crack-tip stress field for smaller elements. The material was again modeled via the incompressible, one-term Ogden model with each set of sample parameters identified in Sect. 2.2.

The cohesive elements were prescribed a bilinear traction-separation law. This traction-separation law is defined such that the cohesive elements have a constant stiffness, E, until the element reaches its peak traction, t_n^o. Beyond this point, the element undergoes damage until it reaches some critical separation, δ^*. The damage, d, which reduces the effective stiffness of the cohesive element is defined as

$$d = \frac{\delta^x(\delta^{max} - \delta^o)}{\delta^{max}(\delta^x - \delta^o)}. \tag{6}$$

Here, δ^{max} is the maximum separation achieved during the loading, δ^o is the separation at the initiation of damage, and δ^x is the separation at which a cohesive element fails. Note that $\delta^* = \delta^x - \delta^o$. We computed G_c for each sample as the area under the traction-separation law curve, see Fig. 4Cii (Good et al. 2020; Patki et al. 2023; Fereidoonnezhad et al. 2021a).

To identify the three parameters of the traction-separation law, i.e., t_n^o, E, and δ^*, we used a least squares approach. That is, we iteratively simulated pure shear experiments of the notched samples up to crack initiation to inform and minimize our objective function defined as

$$\epsilon_t = \gamma\epsilon_f + (1-\gamma)\epsilon_\delta. \tag{7}$$

Here ϵ_t is the total error, $\gamma \in [0, 1]$ is a weight for the error terms, ϵ_f is the error between the experimental and computed force, and ϵ_δ is the error between the experimental and computed critical displacement.

We optimized the weighting factor γ to minimize the overall error. We repeated this inverse analysis for each of our 12 notched pure shear samples to compute their fracture toughness. We used a multistart approach with random initial guesses to minimize the risk of converging to local minima. Also note, this approach did not require the unnotched pure shear sample data or DIC data. Please see Supplementary Table S4 for a list of the cohesive zone parameters for each sample.

3 Results

3.1 Overall fndings

Figure 5 shows the results for all three approaches and the total of six different implementations. Figure 5A compares all implementations of the *Griffith* approach,

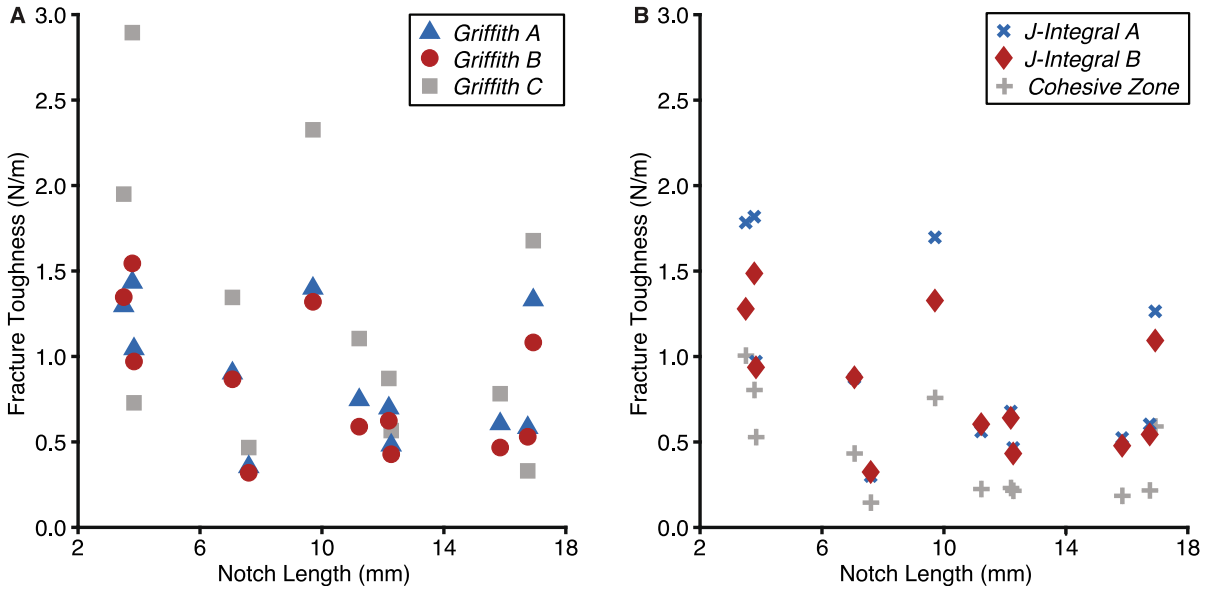

Fig. 5 Fracture toughness values for each approach. **A** Comparisons of the *Griffith* approaches. **B** Comparison of the *J-Integral* approaches and the *cohesive zone* approach

while Fig. 5B compares the *J-Integral* and the *cohesive zone* approaches. Overall, our results suggest that blood clot fracture toughness for our subject ranges from 0.2 N/m to 2.9 N/m with an overall mean of 0.9 $\pm$ 0.54 N/m.

3.2 Consistency

Most notably, the means and the intra-approach variability (as measured by standard deviation) significantly differ between approaches, see Table 1. That is, *Griffith A*, *B*, and *C* yielded means of 0.9 $\pm$ 0.38, 0.8 $\pm$ 0.41, and 1.3 $\pm$ 0.81 N/m, respectively. The *J-Integral* approaches *A* and *B* yielded means of 0.8 $\pm$ 0.39 and 1.0 $\pm$ 0.55 N/m. Finally, the *cohesive zone* approach yielded a mean of 0.5 $\pm$ 0.29 N/m. Among these approaches, the *cohesive zone* approach stands out as having provided estimates that were significantly smaller than the overall mean, while the *Griffith C* approach stands out as having provided estimates that were significantly larger than the overall mean. The remainder of the approaches provided remarkably similar results. Most notably, *Griffith A* and *B* as well as *J-Integral A* deviated the least from the overall mean, i.e., had the smallest inter-approach variability, while also having the smallest standard deviations, i.e., having the smallest intra-approach variability (with the exception of the *cohesive zone* approach that had the smallest overall intra-test variability).

Table 1 Consistency of each approach measured as inter- and intra-approach variability via the mean and standard deviation (Std) and use of additional data

Approach	Mean (N/m)	Std (N/m)	Additional data use		
			DIC	FE	UN
Griffith A	0.9	0.38	–	–	x
Griffith B	0.8	0.41	–	x	–
Griffith C	1.3	0.81	–	–	–
J-Integral A	0.8	0.39	x	x	–
J-Integral B	1.0	0.55	–	x	–
Cohesive zone	0.5	0.29	–	x	–
Overall	0.9	0.54			

DIC Digital image correlation, *FE* finite element, *UN* unnotched samples

3.3 Implementation complexity

Among the six implementations, *Griffith A* stood out as being the least complex to implement. Aside from force, displacement, and imaging data, no numerical or advanced image analyses were required. However,

both notched and unnotched pure shear experiments were required. Next ranks *Griffith C* that required only the implementation of a finite difference scheme, which we did in MATLAB (Mathworks, Natick, MA, USA, Version 2023b). Notably, this approach did not require unnotched pure shear experiments. *Griffith B* ranks third as it required conducting an inverse finite element simulation, but did not require advanced image analyses or additional unnotched pure shear experiments. Tied in third, is the *J-Integral B* approach, which also required an inverse approach and also did not require advanced image analyses or additional unnotched pure shear experiments. Second to last ranks the *J-Integral A* approach that required custom implementations of the J-Integral, sample speckling, and advanced image analyses. We rank the *cohesive zone* approach last as it required an additional inverse finite element simulation, careful consideration of the traction-separation law, and additional sensitivity and convergence studies. Also, regular failure of numerical convergence required manual interventions and repeated executions.

3.4 Computational cost

Our third comparison is by computational cost. Table 2 compares per-sample run times between all methods. Here *Griffith* A and C rank first as they required nearly no computational cost (<1 s), followed by the *Griffith B* and *J-Integral B* methods. Both required inverse finite element analyses to estimate material parameters, but were otherwise inexpensive. Next ranks the *J-Integral A* approach that required computationally costly DIC analyses and an inverse parameter identification. Finally, the *cohesive zone* approach ranks last as it required two inverse analyses. One to identify the material parameters and one to identify the traction-separation law parameters. Especially the latter was expensive owing to the high cost of cohesive zone simulations in Abaqus. It should be noted that it is the only method that captured crack propagation.

4 Discussion

We set out to compare three different approaches (and their six different implementations) to determine the fracture toughness of soft materials. We compared and ranked them by inter- and intra-approach variability, complexity of implementation, and computational cost.

Table 2 Computational cost of each approach

	Run time (s)			
	DIC	Parameter identification	Approach	Total
Griffith A	–	–	<1	<1
Griffith B	–	720	14	734
Griffith C	–	–	<1	<1
J-Integral A	1655	720	15	2390
J-Integral B	–	720	18	738
Cohesive zone	–	720	36,000	36,720

All analyses and simulations were run on 12 intel core i5-10505 processors

4.1 #1 - *Griffith A*

We rank the *Griffith A* approach highest as it provided low inter- and intra-approach variability, was easy to implement, and was of low computational cost. Its only potential down-side is that it requires conducting both unnotched and notched pure shear experiments. Others have chosen to use this method in soft materials for these reasons (Shrimali and Lopez-Pamies 2023; Zhu et al. 2024; Long and Hui 2016).

4.2 #2 - *Griffith B*

Especially for those that have limited access to test specimen, the *Griffith B* approach may be ideal. Although it requires some expertise in finite element simulation, it does not require unnotched pure shear experiments and has comparable intra- and inter-approach variability to our first pick. Thus, for those with finite element expertise, this may be a great alternative.

4.3 #3 - *J-Integral B*

Closely following in the footsteps of *Griffith B* is the *J-Integral B* approach. Again, it provides good intra- and inter-approach variability. This approach also requires minimal implementation complexity and does not require additional unnotched pure shear experiments.

4.4 #4 - *J-Integral A*

This approach ranks relatively low because of its high implementation complexity – requiring sample speckling, DIC, and custom code to evaluate the J-Integral and the high cost of the DIC analysis. Note, this method does not require unnotched pure shear experiments.

4.5 #5 - *Griffith C*

This approach ranks low as it showed high inter- and intra-approach variability. We suspect this variability stems from this approach's raw dependence on experimental data without physical constraint. That is, all other approaches incorporate assumptions about the underlying physics, and/or constraints to specific material behavior, which may help in bounding their error.

4.6 #6 - *Cohesive zone*

The *cohesive zone* approach ranks the lowest because it had high inter-approach variability, was difficult to implement, and was highly computationally expensive. Interestingly, it did show the lowest intra-approach variability. Potential sources for it failing lie in its procedural complexity.

4.7 Limitations

This study is not without limitations. Most importantly, all our approaches assumed that our material behaved purely elastically. Thus, we ignored the material's visco-plastic behavior as well as damage that may contribute to energy dissipation. Future studies should explore the impact of these simplifications on estimating fracture toughness. As we mentioned previously, blood clots may be compressible (Garyfallogiannis et al. 2023). However, during our tests, we did not notice significant fluid expulsion. This supports our analysis of blood clots as an incompressible material. Nonetheless, the reader should keep this limitation in mind when interpreting our findings, and future studies may explore the accrued error when estimating the inherent fracture toughness of blood clot. We also note that there are discrepancies between our DIC-based stress estimates and those predicted by our finite element simulations. Those discrepancies are most evident when comparing Figs. 2B , 3Aiii and Biii. Clearly, our DIC-based stress maps show elevated stresses in the interior of the sample when compared to the numerical results. Those discrepancies most likely stem from our mounting technique in which some Velcro may extend into our sample bulk (Sugerman et al. 2021). As a consequence, our samples behave stiffer close to the boundaries, thus increasing the strain to the interior of the samples. Interestingly, our evaluation techniques appear relatively insensitive to these discrepancies. We suggest that this insensitivity stems from the energetic nature of fracture toughness as a metric. That is, as long as the predicted/measured stored energy (and released energy) between approaches are similar, our fracture toughness calculations will yield similar results. Finally, we limited ourselves to one sample geometry, that of pure shear. We expect our findings can be extended to other geometries as well, but future studies will have to test this assumption.

5 Conclusion

In conclusion, we recommend using the *Griffith A* approach as per the work of Rivlin and Thomas from 1953. It is not without a sense of irony and awe that we make this recommendation, as 70 years of numerical method development and advancements in imaging technology have apparently not improved our ability to estimate fracture toughness from pure shear experiments. We hope others will benefit from our work as they aim to study and understand the fracture behavior of soft materials.

Author contributions M.L. conducted the numerical experiments, prepared the figures, and wrote the manuscript. G.B. conducted all experiments. B.D. helped with the conceptualization and editing of the manuscript. M.R. edited the figures and the manuscript, supervised the numerical and physical experiments, and solicited funding support for this work.

Data avalability Data is openly available on the Texas Data Repository under: https://dataverse.tdl.org/dataverse/DeterminingFractureToughnessData

Declarations

Conflict of interest The authors declare no Conflict of interest.

References

Ang I, Liu Z, Kim J, Hui C-Y, Bouklas N (2020) Effect of elastocapillarity on the swelling kinetics of hydrogels. J Mech Phys Solids 145:104132. https://doi.org/10.1016/j.jmps.2020.104132

Barenblatt G (1962) The mathematical theory of equilibrium cracks in brittle fracture. Adv Appl Mech 7:55–129

Blaber J, Adair B, Antoniou A (2015) Ncorr: open-source 2d digital image correlation matlab software. Exp Mech 55(6):1105–1122. https://doi.org/10.1007/s11340-015-0009-1

Bouklas N, Landis CM, Huang R (2015) Effect of solvent diffusion on crack-tip fields and driving force for fracture of hydrogels. J Appl Mech 82:081007. https://doi.org/10.1115/1.4030587

Chen C, Wang Z, Suo Z (2017) Flaw sensitivity of highly stretchable materials. Extrem Mech Lett 10:50–57. https://doi.org/10.1016/j.eml.2016.10.002

Crespo-Cuevas V, Ferguson VL, Vernerey F (2023) Poroviscoelasto-plasticity of agarose-based hydrogels. Soft Matter 19:790–806. https://doi.org/10.1039/D2SM01356H

Dortdivanlioglu B, Javili A (2021) Boundary viscoelasticity theory at finite deformations and computational implementation using isogeometric analysis. Comput Methods Appl Mech Eng 374:113579. https://doi.org/10.1016/j.cma.2020.113579

Dortdivanlioglu B, Javili A (2022) Plateau Rayleigh instability of soft elastic solids. Effect of compressibility on pre and post bifurcation behavior. Extrem Mechan Lett 55:101797. https://doi.org/10.1016/j.eml.2022.101797

Dortdivanlioglu B, Linder C (2019) Diffusion-driven swelling-induced instabilities of hydrogels. J Mech Phys Solids 125:38–52. https://doi.org/10.1016/j.jmps.2018.12.010

Dugdale D (1960) Yielding of steel sheets containing slits. J Mech Phys Solids 8(2):100–104. https://doi.org/10.1016/0022-5096(60)90013-2

Fereidoonnezhad B, Dwivedi A, Johnson S, McCarthy R, McGarry P (2021) Blood clot fracture properties are dependent on red blood cell and fibrin content. Acta Biomater 127:213–228. https://doi.org/10.1016/j.actbio.2021.03.052

Fereidoonnezhad B, Moerman KM, Johnson S, McCarthy R, McGarry PJ (2021) A new compressible hyperelastic model for the multi-axial deformation of blood clot occlusions in vessels. Biomech Model Mechanobiol 20(4):1317–1335. https://doi.org/10.1007/s10237-021-01446-4

Fung Y-C (1993) Biomechanics, 2nd edn. Springer, New York

Garyfallogiannis K, Ramanujam RK, Litvinov RI, Yu T, Nagaswami C, Bassani JL, Weisel JW, Purohit PK, Tutwiler V (2023) Fracture toughness of fibrin gels as a function of protein volume fraction: mechanical origins. Acta Biomater 159:49–62. https://doi.org/10.1016/j.actbio.2022.12.028

Ghezelbash F, Liu S, Shirazi-Adl A, Li J (2022) Blood clot behaves as a poro-visco-elastic material. J Mech Behav Biomed Mater 128:105101. https://doi.org/10.1016/j.jmbbm.2022.105101

Good BC, Simon S, Manning K, Costanzo F (2020) Development of a computational model for acute ischemic stroke recanalization through cyclic aspiration. Biomech Model Mechanobiol 19(2):761–778. https://doi.org/10.1007/s10237-019-01247-w

Griffith AA (1921) VI. the phenomena of rupture and flow in solids, Philosophical Transactions of the Royal Society of London. Series A, Containing Papers of a Mathematical or Physical Character 221(582):163–198. https://doi.org/10.1098/rsta.1921.0006

Gültekin O, Lohr MJ, Bechtel GN, Rausch MK (2024) "What makes blood clots break off?" A back-of-the-envelope computation toward explaining clot embolization. Cardiovasc Eng Technol. https://doi.org/10.1007/s13239-024-00733-2

Kim DH, Lu N, Ma R, Kim Y-S, Kim R-H, Wang S, Wu J, Won SM, Tao H, Islam A, Yu KJ, Kim T-I, Chowdhury R, Ying M, Xu L, Li M, Chung H-J, Keum H, McCormick M, Liu P, Zhang Y-W, Omenetto FG, Huang Y, Coleman T (2011) Rogers, epidermal electronics. Science 333:838–843

Knowles JK, Sternberg E (1973) An asymptotic finite-deformation analysis of the elastostatic field near the tip of a crack. J Elast 3(2):67–107. https://doi.org/10.1007/BF00045816

Lee KY, Mooney DJ (2001) Hydrogels for tissue engineering. Chem Rev 101(7):1869–1880. https://doi.org/10.1021/cr000108x

Li E, Zhang Z, Chang CC, Liu GR, Li Q (2015) Numerical homogenization for incompressible materials using selective smoothed finite element method. Compos Struct 123:216–232. https://doi.org/10.1016/j.compstruct.2014.12.016

Liu S, Bao G, Ma Z, Kastrup CJ, Li J (2021) Fracture mechanics of blood clots: measurements of toughness and critical length scales. Extrem Mech Lett 48:101444. https://doi.org/10.1016/j.eml.2021.101444

Lohr MJ, Sugerman GP, Kakaletsis S, Lejeune E, Rausch MK (2022) An introduction to the ogden model in biomechanics: benefits, implementation tools and limitations, philosophical transactions of the royal society A: mathematical. Phys Eng Sci 380(2234):20210365. https://doi.org/10.1098/rsta.2021.0365

Long R, Hui C-Y (2015) Crack tip fields in soft elastic solids subjected to large quasi-static deformation - a review. Extreme Mech Lett 4:131–155. https://doi.org/10.1016/j.eml.2015.06.002

Long R, Hui C-Y (2016) Fracture toughness of hydrogels: measurement and interpretation. Soft Matter 12(39):8069–8086. https://doi.org/10.1039/C6SM01694D

Luraghi G, Rodriguez Matas JF, Dubini G, Berti F, Bridio S, Duffy S, Dwivedi A, McCarthy R, Fereidoonnezhad B, McGarry P, Majoie CBLM, Migliavacca F (2021) on behalf of the INSIST investigators, Applicability assessment of a stent-retriever thrombectomy finite-element model, interface. Focus 11(1):20190123. https://doi.org/10.1098/rsfs.2019.0123

Luraghi G, Bridio S, Rodriguez Matas JF, Dubini G, Boodt N, Gijsen FJ, Van Der Lugt A, Fereidoonnezhad B, Moerman KM, McGarry P, Konduri PR, Arrarte Terreros N, Marquering HA, Majoie CB, Migliavacca F (2021) The first virtual patient-specific thrombectomy procedure. J Biomech 126:110622. https://doi.org/10.1016/j.jbiomech.2021.110622

McClements DJ, Decker EA, Park Y, Weiss J (2009) Structural design principles for delivery of bioactive components in nutraceuticals and functional foods. Crit Rev Food Sci Nutr 49(6):577–606. https://doi.org/10.1080/10408390902841529

Mousavi SM, J. S., Faghihi D, Sommer K, Bhurwani MMS, Patel TR, Santo B, Waqas M, Ionita C, Levy EI, Siddiqui AH, Tutino VM, (2021) Realistic computer modelling of stent

retriever thrombectomy: a hybrid finite-element analysis-smoothed particle hydrodynamics model. J Royal Soc Interface 18(185):20210583. https://doi.org/10.1098/rsif.2021.0583

Mullins L (1969) Softening of rubber by deformation. Rubber Chem Technol 42:339–362

Nassar JM, Rojas JP, Hussain AM, Hussain MM (2016) From stretchable to reconfigurable inorganic electronics. Extrem Mech Lett 9:245–268. https://doi.org/10.1016/j.eml.2016.04.011

Ogden RW (1972) Large deformation isotropic elasticity-on the correlation of theory and experiment for incompressible rubberlike solids. Philosoph Trans Royal Soc A: Math phys Eng Sci 326(1567):565–584. https://doi.org/10.1098/rspa.1972.0026

Patki P, Simon S, Manning KB, Costanzo F (2023) Computational analysis of effects of clot length on acute ischemic stroke recanalization under different cyclic aspiration loading conditions. Int J Numerical Methods Biomed Eng 39(2):e3667. https://doi.org/10.1002/cnm.3667

Peppas N, Hilt J, Khademhosseini A, Langer R (2006) Hydrogels in biology and medicine: from molecular principles to bionanotechnology. Adv Mater 18(11):1345–1360. https://doi.org/10.1002/adma.200501612

Perez-Puyana V, Jiménez-Rosado M, Guerrero A, Romero A (2020) Anisotropic properties of PCL/gelatin scaffolds obtained via electrospinning. Int J Fract 224(2):269–276. https://doi.org/10.1007/s10704-020-00460-4

Piggott MR (1975) Fracture: I. brittleness criterion derived from the stability of moderately thin cracks. Int J Fract 11(3):479–488. https://doi.org/10.1007/BF00033534

Qi Y, Zou Z, Xiao J, Long R (2019) Mapping the nonlinear crack tip deformation field in soft elastomer with a particle tracking method. J Mech Phys Solids 125:326–346. https://doi.org/10.1016/j.jmps.2018.12.018

Qiu Y, Myers DR, Lam WA (2019) The biophysics and mechanics of blood from a materials perspective. Nat Rev Mater 4(5):294–311. https://doi.org/10.1038/s41578-019-0099-y

Ramanujam RK, Garyfallogiannis K, Litvinov RI, Bassani JL, Weisel JW, Purohit PK, Tutwiler V (2024) Mechanics and microstructure of blood plasma clots in shear driven rupture. Soft Matter 20(21):4184–4196. https://doi.org/10.1039/D4SM00042K

Rastogi A, Dortdivanlioglu B (2022) Modeling curvature-resisting material surfaces with isogeometric analysis. Comput Methods Appl Mech Eng 401:115649. https://doi.org/10.1016/j.cma.2022.115649

Rice JR (1968) A path independent integral and the approximate analysis of strain concentration by notches and cracks. J Appl Mech 35(2):379–386. https://doi.org/10.1115/1.3601206

Rivlin RS, Thomas AG (1953) Rupture of rubber. i. characteristic energy for tearing. J Polym Sci 10(3):291–318. https://doi.org/10.1002/pol.1953.120100303

Robinson A, Nkansah A, Bhat S, Karnik S, Jones S, Fairley A, Leung J, Wancura M, Sacks MS, Dasi LP, Cosgriff-Hernandez E (2024) Hydrogel-polyurethane fiber composites with enhanced microarchitectural control for heart valve replacement. J Biomed Mater Res, Part A 112(4):586–599. https://doi.org/10.1002/jbm.a.37641

Roucou D, Diani J, Brieu M (2015) Critical strain energy release rate for rubbers: single edge notch tension vs. pure shear tests. Int J Fract 209:163–170. https://doi.org/10.1007/s10704-018-00336-8

Shrimali B, Lopez-Pamies O (2023) The "pure-shear" fracture test for viscoelastic elastomers and its revelation on griffith fracture. Extreme Mech Lett 58:101944. https://doi.org/10.1016/j.eml.2022.101944

Shur M, Akouissi O, Rizzo O, Colin DJ, Kolinski JM, Lacour SP (2023) Revealing the complexity of ultra-soft hydrogel re-swelling inside the brain. Biomaterials 294:122024. https://doi.org/10.1016/j.biomaterials.2023.122024

Slaughter BV, Khurshid SS, Fisher OZ, Khademhosseini A, Peppas NA (2009) Hydrogels in regenerative medicine. Adv Mater 21(32):3307–3329. https://doi.org/10.1002/adma.200802106

Stano G, Percoco G (2021) Additive manufacturing aimed to soft robots fabrication: A review. Extrem Mech Lett 42:101079. https://doi.org/10.1016/j.eml.2020.101079

Style RW, Jagota A, Hui C-Y, Dufresne ER (2017) Elastocapillarity: surface tension and the mechanics of soft solids. Ann Rev Condens Matter Phys 8:99–118. https://doi.org/10.1146/annurev-conmatphys-031016-025326

Sugerman GP, Parekh SH, Rausch MK (2020) Nonlinear, dissipative phenomena in whole blood clot mechanics. Soft Matter 16(43):9908–9916. https://doi.org/10.1039/D0SM01317J

Sugerman GP, Chokshi A, Rausch MK (2021) Preparation and mounting of whole blood clot samples for mechanical testing. Curr Protocols 1(7):e197. https://doi.org/10.1002/cpz1.197

Sugerman GP, Kakaletsis S, Thakkar P, Chokshi A, Parekh SH, Rausch MK (2021) A whole blood thrombus mimic: constitutive behavior under simple shear. J Mech Behav Biomed Mater 115:104216. https://doi.org/10.1016/j.jmbbm.2020.104216

Sugerman GP, Yang J, Rausch MK (2023) A speckling technique for DIC on ultra-soft, highly hydrated materials. Exp Mech 63(3):585–590. https://doi.org/10.1007/s11340-023-00938-x

Sugerman GP, Bechtel GN, Malinowska Z, Parekh SH, Rausch MK (2024) Mechanical properties of clot made from human and bovine whole blood differ significantly. J Mech Behav Biomed Mater 154:106508. https://doi.org/10.1016/j.jmbbm.2024.106508

Sun J-Y, Zhao X, Illeperuma WRK, Chaudhuri O, Oh KH, Mooney DJ, Vlassak JJ, Suo Z (2012) Highly stretchable and tough hydrogels. Nature 489(7414):133–136. https://doi.org/10.1038/nature11409

Tutwiler V, Singh J, Litvinov RI, Bassani JL, Purohit PK, Weisel JW (2020) Rupture of blood clots: mechanics and pathophysiology. Sci Adv 6(35):eabc0496. https://doi.org/10.1126/sciadv.abc0496

Varner H, Sugerman GP, Rausch MK, Cohen T (2023) Elasticity of whole blood clots measured via volume controlled cavity expansion. J Mech Behav Biomed Mater 143:105901. https://doi.org/10.1016/j.jmbbm.2023.105901

Wang Q, Zhao X (2015) A three-dimensional phase diagram of growth-induced surface instabilities. Sci Rep 5:8887. https://doi.org/10.1038/srep08887

Wei X, Li C, McCarthy C, Kolinski JM (2024) Complexity of crack front geometry enhances toughness of brit-

tle solids. Nat Phys 20:1009–1014. https://doi.org/10.1038/s41567-024-02435-x

Wendelboe AM, Raskob GE (2016) Global burden of thrombosis: epidemiologic aspects. Circ Res 118(9):1340–1347. https://doi.org/10.1161/CIRCRESAHA.115.306841

Xu L, Wagner RJ, Liu S, He Q, Li T, Pan W, Feng Y, Feng H, Meng Q, Zou X, Fu Y, Shi X, Zhao D, Ding J, Vernerey FJ (2022) Locomotion of an untethered, worm-inspired soft robot driven by a shape-memory alloy skeleton. Sci Rep 12(1):12392. https://doi.org/10.1038/s41598-022-16087-5

Yang CH, Chen B, Lu JJ, Yang JH, Zhou J, Chen YM, Suo Z (2015) Ionic cable. Extrem Mech Lett 3:59–65. https://doi.org/10.1016/j.eml.2015.03.001

Yoda R (1998) Elastomers for biomedical applications. J Biomater Sci Polym Ed 9(6):561–626. https://doi.org/10.1163/156856298X00046

Zhou B, Rachev A, Shazly T (2015) The biaxial active mechanical properties of the porcine primary renal artery. J Mech Behav Biomed Mater 48:28–37. https://doi.org/10.1016/j.jmbbm.2015.04.004

Zhu B, Wang J, Zehnder AT, Hui C-Y (2024) Energy release rate of a mode-i crack in pure shear specimens subjected to large deformation. Int J Fract 245(3):171–182. https://doi.org/10.1007/s10704-023-00751-6